

INFORMATION TO USERS

This was produced from a copy of a document sent to us for microfilming. While the most advanced technological means to photograph and reproduce this document have been used, the quality is heavily dependent upon the quality of the material submitted.

The following explanation of techniques is provided to help you understand markings or notations which may appear on this reproduction.

1. The sign or "target" for pages apparently lacking from the document photographed is "Missing Page(s)". If it was possible to obtain the missing page(s) or section, they are spliced into the film along with adjacent pages. This may have necessitated cutting through an image and duplicating adjacent pages to assure you of complete continuity.
2. When an image on the film is obliterated with a round black mark it is an indication that the film inspector noticed either blurred copy because of movement during exposure, or duplicate copy. Unless we meant to delete copyrighted materials that should not have been filmed, you will find a good image of the page in the adjacent frame.
3. When a map, drawing or chart, etc., is part of the material being photographed the photographer has followed a definite method in "sectioning" the material. It is customary to begin filming at the upper left hand corner of a large sheet and to continue from left to right in equal sections with small overlaps. If necessary, sectioning is continued again—beginning below the first row and continuing on until complete.
4. For any illustrations that cannot be reproduced satisfactorily by xerography, photographic prints can be purchased at additional cost and tipped into your xerographic copy. Requests can be made to our Dissertations Customer Services Department.
5. Some pages in any document may have indistinct print. In all cases we have filmed the best available copy.

University
Microfilms
International

300 N. ZEEB ROAD, ANN ARBOR, MI 48106
18 BEDFORD ROW, LONDON WC1R 4EJ, ENGLAND

FREUND, GEORGE ANTON, JR.

RAMAN SCATTERING FROM MIXED-CRYSTAL LAYERED COMPOUNDS

The University of Nebraska - Lincoln

PH.D.

1979

University
Microfilms
International

300 N. Zeeb Road, Ann Arbor, MI 48106

18 Bedford Row, London WC1R 4EJ, England

Copyright 1980

by

Freund, George Anton, Jr.

All Rights Reserved

PREVIEW

RAMAN SCATTERING FROM MIXED-CRYSTAL LAYERED COMPOUNDS

by

George A. Freund, Jr.

A DISSERTATION

Presented to the Faculty of

The Graduate College in the University of Nebraska

In Partial Fulfillment of Requirements

For the Degree of Doctor of Philosophy

Major: Physics

Under the Supervision of Associate Professor Roger D. Kirby

Lincoln, Nebraska

December, 1979

TITLE

RAMAN SCATTERING FROM MIXED-CRYSTAL

LAYERED COMPOUNDS

BY

George A. Freund, Jr.

APPROVED

DATE

Roger D. Kirby

November 15, 1979

John R. Hardy

November 15, 1979

Edgar A. Pearlstein

November 15, 1979

Edward J. Zimmerman

November 15, 1979

SUPERVISORY COMMITTEE

GRADUATE COLLEGE

UNIVERSITY OF NEBRASKA

RAMAN SCATTERING FROM MIXED-CRYSTAL LAYERED COMPOUNDS

George A. Freund, Jr., Ph.D.

University of Nebraska, 1979

Advisor: Roger D. Kirby

Reported here are results of Raman scattering experiments on mixed crystals related to the transition metal dichalcogenide TiSe_2 : $\text{TiSe}_{2-x}\text{S}_x$, $\text{TiSe}_{2-x}\text{Te}_x$, $\text{Zr}_x\text{Ti}_{1-x}\text{Se}_2$, and $\text{V}_x\text{Ti}_{1-x}\text{Se}_2$. Pure TiSe_2 is of interest because it undergoes a displacive structural phase transition to a superlattice. The mechanism for this phase transition is a matter of some debate. There are two main aspects of the results reported here: 1) the mixed crystal lattice dynamics, and 2) the mechanism for the superlattice formation in TiSe_2 , including the effect of doping upon the transition.

Two Raman-active phonons, one A_{1g} and one doubly degenerate E_g , are predicted by group theory for the undistorted TiSe_2 structure. The frequencies of these phonons were measured in the above four mixed-crystal systems. In $\text{TiSe}_{2-x}\text{Te}_x$, these phonons follow a one-mode behavior and this is modelled in a virtual-crystal approximation. The agreement between the observed and calculated frequencies is excellent.

On the other hand, in $\text{TiSe}_{2-x}\text{S}_x$ and $\text{Zr}_x\text{Ti}_{1-x}\text{Se}_2$, there is a two-mode behavior; that is, an additional mode of A_{1g} symmetry appears in the Raman spectrum. A lattice-dynamical model involving short-range forces has been reformulated in the

random-element isodisplacement approximation in an attempt to model this behavior. The agreement between the observed and calculated frequencies is better for the A_{1g} modes than for the E_g modes in $\text{TiSe}_{2-x}\text{S}_x$ but for $\text{Zr}_x\text{Ti}_{1-x}\text{Se}_2$ the model fails to predict a two-mode behavior although it does correctly predict the A_{1g} and E_g mode frequencies. In $\text{TiSe}_{2-x}\text{S}_x$ at $x = 0.80$, there is an abrupt discontinuity in the frequency of the higher frequency A_{1g} mode as a function of x , after which the two-mode behavior disappears. This is interpreted to be a result of the transformation from semimetal to semiconductor, which must occur in this system.

Data on the $\text{V}_x\text{Ti}_{1-x}\text{Se}_2$ mixed crystals were obtained only at relatively low concentrations, so there is insufficient evidence to determine whether the phonons in this system follow a one-mode or a two-mode behavior.

Several mechanisms have been proposed as the cause of the superlattice formation in TiSe_2 , including electron-hole interactions and the softening of a zone-boundary phonon. Evidence for the formation of a superlattice below the transition temperature consists of additional peaks in the Raman spectra of the mixed crystals, similar to those observed in pure TiSe_2 below 202 K. In the mixed crystals the frequencies of the superlattice peaks were measured as a function of x . In $\text{TiSe}_{2-x}\text{Te}_x$ and $\text{V}_x\text{Ti}_{1-x}\text{Se}_2$ the phase-transition temperature decreases rapidly for $x \leq 0.10$, while in $\text{TiSe}_{2-x}\text{S}_x$ and $\text{Zr}_x\text{Ti}_{1-x}\text{Se}_2$ the superlattice persists to higher doping levels. The combination of the data presented here, with the results of band structure calculations and other experimental

data on these and related systems, support the view that the superlattice formation is the result of an electronic instability which depends critically on the balance of the concentration of electrons in the conduction band and holes in the valence band. However, the soft-phonon mechanism cannot be completely ruled out.

PREVIEW

ACKNOWLEDGEMENTS

I wish to thank Roger Kirby for his suggestion of this research topic, for his encouragement, for his assistance, for his insight, for his advice, and most of all for his patience.

I am grateful to Professors Ed Pearlstein and John Hardy for their critical reading of this dissertation and their helpful suggestions. In addition, I have enjoyed stimulating discussions with them as well as Professors Sitaram Jaswal and John Weymouth and Doctors James Duffey, Joel Gerber, and Shahid Haque. I also thank Wes Nieveen for his help in the crystal growth laboratory and Don Galliardt for his help with the minicomputer system.

I thank department chairmen, Professors Dave Sellmyer and Leo Sartori for support through teaching assistantships. I also thank NSF for travel funds and support under grant DMR 77-10217.

I am grateful to Mrs. Marj Golter for her fast and accurate typing of this dissertation.

I thank my parents and my in-laws for their encouragement, help with babysitting, and various other activities so that I could pursue these studies.

Finally and most importantly, I want to thank my wife Pat for the sacrifices she has made during our years here in Nebraska. Without her support, encouragement, patience and love I could never have finished this degree program. I also thank my children Paul, Michael, and Rachel for enduring my prolonged absences from home and any other hardships I may have caused them.

TABLE OF CONTENTS

	<u>Page</u>
ABSTRACT.	<i>i</i>
ACKNOWLEDGEMENTS.	<i>iv</i>
TABLE OF CONTENTS	<i>v</i>
LIST OF FIGURES	<i>viii</i>
LIST OF TABLES.	<i>xi</i>
CHAPTER 1. Introduction.	1
CHAPTER 2. Titanium Dichalcogenide Samples	7
A. Crystallography	7
B. Stoichiometry	9
C. Crystal Growth.	13
D. Crystal Characterization.	18
CHAPTER 3. Raman Spectra of the Mixed Crystals	22
A. Introduction.	22
B. Experimental Considerations	26
1) Raman Scattering Apparatus	26
a) Light Source.	27
b) Spectrometer.	27
c) Detector.	28
d) Data Acquisition System	29
2) Special Considerations	29
a) Scattering from Metals.	29
b) Low and High Temperature Measurements	33
c) Polarization Measurements	36
C. Results	37
1) Anion-doped Samples.	37
a) $\text{TiSe}_{2-x}\text{S}_x$	38
b) $\text{TiSe}_{2-x}\text{Te}_x$	50
2) Cation-doped Samples	53
a) $\text{Zr}_x\text{Ti}_{1-x}\text{Se}_2$	53
b) $\text{V}_x\text{Ti}_{1-x}\text{Se}_2$	57
D. Summary	57

	<u>Page</u>
CHAPTER 4. Mixed-Crystal Lattice Dynamics.	60
A. Introduction.	60
B. Anion-doped Mixed Crystals.	65
1) $\text{TiSe}_2\text{-}_x\text{Te}_x$ and Virtual Crystal Approximation	66
2) $\text{TiSe}_2\text{-}_x\text{S}_x$	68
3) The Random Element Isodisplacement Model	68
4) Jaswal's Lattice Dynamical Model and Random Element Isodisplacement Calculation for $\text{TiSe}_2\text{-}_x\text{S}_x$	73
C. $\text{Zr}_x\text{Ti}_{1-x}\text{Se}_2$ Mixed Crystals.	81
D. Discussion.	86
1) Semimetal-to-Semiconductor Transformation in $\text{TiSe}_2\text{-}_x\text{S}_x$ and $\text{Zr}_x\text{Ti}_{1-x}\text{Se}_2$	86
2) Calculations	88
3) A Symmetry Argument.	91
4) Comments on the Random Element Isodisplacement Model	94
CHAPTER 5. Superlattice Formation in the Mixed Crystals. . .	97
A. Introduction.	97
B. Anion-doped Mixed Crystals.	107
1) $\text{TiSe}_2\text{-}_x\text{S}_x$	107
2) $\text{TiSe}_2\text{-}_x\text{Te}_x$	109
C. Cation-doped Mixed Crystals	111
1) $\text{Zr}_x\text{Ti}_{1-x}\text{Se}_2$	111
2) $\text{V}_x\text{Ti}_{1-x}\text{Se}_2$	111
D. Discussion.	112
1) Effect of Doping on Superlattice Formation	112
2) Band Structure Calculations.	113
3) Proposed Mechanisms.	115
a) Band Pseudo-Jahn-Teller Effect.	116
b) Soft Phonon Mode.	117
c) Susceptibility Peaks and Changing Bond Lengths.	119
d) Excitonic Insulator Model	123
CHAPTER 6. Summary	126

	<u>Page</u>
APPENDIX I. X-ray Lattice Parameter Measurements	131
APPENDIX II. Raman Scattering	142
A. Preliminary Background	142
B. Quantum Mechanical Derivation.	146
1) The Raman Scattered Intensity	146
2) Temperature Dependence.	155
3) Resonance Effects	156
4) Applications.	157
C. Selection Rules and Symmetry	158
APPENDIX III. Transition Metal Monochalcogenides	162
A. NiS.	162
B. FeS.	175
C. Discussion	181
REFERENCES.	183

LIST OF FIGURES

<u>Figure</u>		<u>Page</u>
2-1	The 1T-Polytype Layered Compound	8
2-2	The NiAs and CdI_2 Structures	10
3-1	The Brillouin Zone of TiSe_2	23
3-2	Zone-center Normal Mode Displacement Patterns for Undistorted TiSe_2	24
3-3	The Raman Scattering System.	28
3-4	The Raman Scattering Geometry.	32
3-5	The Liquid Nitrogen Exchange Gas Cryostat and Sample Probe	35
3-6	The $(x', \frac{x}{y})$ Raman Spectrum of TiS_2	39
3-7	Polarization Analyzed Raman Spectra of TiS_2	41
3-8	The $(x', \frac{x}{y})$ Raman Spectrum of TiSe_2	43
3-9	Representative Spectra of the $\text{TiSe}_{2-x}\text{S}_x$ System ($x = 0, 0.1, 0.4, 0.8$)	44
3-10	Representative Spectra of the $\text{TiSe}_{2-x}\text{S}_x$ System ($x = 1.2, 1.6, 1.8, 2.0$)	45
3-11	Raman Spectra of $\text{TiSe}_{2-x}\text{S}_x$ for $0.60 \leq x \leq 0.80$	47
3-12	Low Temperature Raman Spectra of $\text{TiSe}_{2-x}\text{S}_x$ ($x = 0.2, 0.4, 0.6$).	48
3-13	Representative Raman Spectra of the $\text{TiSe}_{2-x}\text{Te}_x$ System ($x = 2.0, 1.8, 1.6, 1.4$)	51
3-14	Representative Raman Spectra of the $\text{TiSe}_{2-x}\text{Te}_x$ System ($x = 2.0, 1.8, 1.6, 1.4$)	52
3-15	Representative Spectra of the $\text{Zr}_x\text{Ti}_{1-x}\text{Se}_2$ System ($x = 0.02; 0.03, 0.10, 0.12, 0.15$)	54

<u>Figure</u>	<u>Page</u>
3-16 Detailed View of $\text{Zr}_x\text{Ti}_{1-x}\text{Se}_2$ Spectra ($x = 0.02$ and $x = 0.03$)	55
3-17 Raman Spectra of $\text{V}_x\text{Ti}_{1-x}\text{Se}_x$ ($x = 0.02$ and $x = 0.05$)	58
4-1 Virtual Crystal Calculation for $\text{TiSe}_{2-x}\text{Te}_x$	67
4-2 Virtual Crystal Calculation for $\text{TiSe}_{2-x}\text{S}_x$	69
4-3 Diatomic Linear Chain.	71
4-4 Mixed Diatomic Linear Chain in Random Element Isodisplacement Model.	72
4-5 Short-Range Interatomic Force Constants.	74
4-6 Random Element Isodisplacement Calculations for $\text{TiSe}_{2-x}\text{S}_x$ - A-like Modes	78
4-7 Random Element Isodisplacement Calculations for $\text{TiSe}_{2-x}\text{S}_x$ - E-like Modes	79
4-8 Random Element Isodisplacement Calculations for $\text{Zr}_x\text{Ti}_{1-x}\text{Se}_2$ - A-like Modes	83
4-9 Random Element Isodisplacement Calculations for $\text{Zr}_x\text{Ti}_{1-x}\text{Se}_2$ - E-like Modes	84
4-10 A_{1g} Symmetry Vibrations Around a Metal Impurity Site.	92
5-1 Fermi Surfaces of Some Layered Compounds	105
5-2 Low Temperature Frequencies of $\text{TiSe}_{2-x}\text{S}_x$ as a Function of x	108
5-3 Transition Temperature as a Function of Per Cent Dopant.	110

<u>Figure</u>	<u>Page</u>
I-1 c' versus $f(\theta)$ for $\text{TiSe}_{1.6}\text{S}_{0.4}$	133
I-2 (004) Bragg Diffraction Peak for $\text{TiSe}_{1.2}\text{S}_{0.8}$	135
I-3 c versus x for $\text{TiSe}_{2-x}\text{S}_x$	138
II-1 Energy Level Diagram for Simple Scattering Processes.	152
III-1 The Unit Cell of NiS	165
III-2 Infrared- and Raman-active Normal Mode Displacement Patterns for NiS	168
III-3 Displacement Patterns of the E_2 Modes of NiS in the Assumed Distorted Structure.	171
III-4 Relative Resistivity versus Temperature for NiS	174
III-5 Logarithm of Voltage versus $1/T$ for FeS	180

LIST OF TABLES

	<u>Page</u>
2-1 List of Samples Studied, Growth Temperature Distribution and Starting Materials.	16
3-1 Low Temperature Raman Lines of $\text{TiSe}_{2-x}\text{S}_x$ ($x = 0, 0.2, 0.4, 0.6$).	49
4-1 Phonon Frequencies for the Anion-Doped Mixed Crystal Calculations	79
4-2 Phonon Frequencies for the Cation-Doped Mixed Crystal Calculations	85
4-3 Correlation Diagram for Metal Impurity in TiSe_2 . . .	93
I-1 Measurements of the c Lattice Constant	139
II-1 Theorems Important to Raman Scattering	160
III-1 Correlation Diagram for NiAs Structure	167
III-2 Correlation Diagram for Assumed Distorted NiS Structure.	170
III-3 Correlation Diagram for Distorted FeS Structure.	177

CHAPTER 1

INTRODUCTION

The transition metals and transition metal compounds exhibit a wide variety of physical properties ranging from superconductivity^{1,2}, ferromagnetism³ and antiferromagnetism⁴, to a variety of structural and electronic instabilities such as, metal-to-non-metal transitions⁴, and charge-⁵ and spin-⁶ density waves. This range of properties is largely a consequence of slight differences in the d-band electronic structure of these compounds.⁷⁻⁹ The transition-metal dichalcogenides (MX_2 , M = transition metals of groups IVb, Vb, and VIb; X = S, Se, or Te) and their mixed crystals (or solid solutions) are the subject of particular interest in this dissertation. These compounds grow in quasi-two-dimensional layered structures, with strong covalent or metallic bonds within the layers and much weaker van der Waals bonds between the layers⁸. As a consequence of the bonding, these crystals have a highly anisotropic character, their properties parallel to the layers being significantly different from those perpendicular to the layers. In the last ten to fifteen years the transition-metal dichalcogenides have come under increasing scrutiny: first, for their anomalous optical and electronic properties⁸, then, as possible systems in which to observe "excitonic superconductivity"¹⁰, and most recently because they

exhibit phase transitions to structurally distorted states at low temperatures⁵. The investigation of such phase transitions is of major concern in this dissertation.

The phase transitions in the transition-metal dichalcogenides are displacive, structural distortions which cause additional optic phonons to appear at long wavelengths. Since Raman scattering is a sensitive probe for studying long wavelength phonons in solids, it is an ideal technique through which to study the distorted state and its onset. This dissertation reports the Raman scattering measurements on a number of pure and doped layered dichalcogenides. These compounds are particularly fruitful for Raman scattering investigations for several reasons:

- 1) They are very anisotropic and so offer the opportunity to study the lattice dynamics of nearly two-dimensional crystals. While several simple theoretical models have been proposed to describe the lattice dynamics of a few of these materials¹¹⁻¹⁵, experimental data are needed to determine the usefulness and validity of these models and point out modifications that need to be made to them.

- 2) The lattice dynamics of mixed crystals is a topic of current experimental and theoretical interest. In some cases, the $q = 0$ phonons of these mixed crystals are observed to vary monotonically in frequency between the frequencies of the two pure compounds as the concentration of impurities is increased. This is commonly referred to as "one mode" behavior¹⁶. In other cases, an additional long-wavelength mode may appear so

that two modes in the defect system appear in the vicinity of the pure-crystal optic-phonon frequencies. These modes usually vary in frequency as the concentration of impurities is changed. This effect is commonly referred to as "two-mode" behavior¹⁶. A number of approaches to understanding this problem have been tried with limited success, but no comprehensive theory yet exists¹⁶⁻¹⁸. In many cases, mixed crystals of the layered transition-metal dichalcogenides can be grown over a wide range of compositions. The Raman spectra of mixed crystal layered compounds are fairly easy to investigate and a number of interesting features, including one-mode and two-mode behaviors, are reported in this dissertation.

3) While the lattice dynamics of the pure and doped layered compounds is of considerable interest, the most intriguing characteristic of these compounds is that some of them undergo structural phase transitions related to the formation of charge-density waves. A charge-density wave is a static spatial variation in the conduction electron density, with a wavelength typically of a few lattice constants. A variety of experiments have verified the existence of charge-density wave formation in the Vb dichalcogenides, VSe_2 ^{19,20}, NbSe_2 ^{5,21-24}, TaS_2 ^{5,25} and TaSe_2 ^{5,23,24,26,29}. This phenomenon has been reported only in quasi-one-dimensional and quasi-two-dimensional compounds; it has not yet been observed in materials with a strongly three dimensional character. The presently available experimental evidence indicates that the transition to the charge-density

wave state in such limited dimensionality materials is a consequence of their relatively simple Fermi surface geometries. Furthermore, Chan and Heine³⁰ have shown that a transition to a charge-density wave state is necessarily accompanied by a structural distortion of the same wavelength as the charge density wave. Extremely complex Raman spectra are observed in the distorted state. In general, several of these new $q = 0$ phonons are strongly coupled to the charge-density wave, as is indicated by their large Raman intensities and strong temperature dependence near the transition temperature.

Most of the research presented here deals with TiSe_2 , a IVb dichalcogenide which has many physical properties similar to those of the Vb layered compounds described above, including a phase transition to a distorted state at 202 K.³¹⁻³⁶ There are, however, some subtle differences between the behavior of TiSe_2 and that of the Vb compounds. While it seems likely that this distortion is due to a transition to a charge-density-wave state, this has not been proved conclusively. Judging from the models proposed there is some question whether the distortion in TiSe_2 is the result of an electronic instability or a phonon instability.

Raman scattering measurements were made on the pure compounds TiS_2 , TiSe_2 , and TiTe_2 and on the mixed crystal systems $\text{TiSe}_{2-x}\text{S}_x$, $\text{TiSe}_{2-x}\text{Te}_x$, $\text{Zr}_x\text{Ti}_{1-x}\text{Se}_2$, and $\text{V}_x\text{Ti}_{1-x}\text{Se}_2$ in order to obtain information which can lead to better understanding of this 202 K phase transition as well as of the mixed-crystal lattice dynamics. In

particular, dependence of the phase transition on impurity concentration, x , and on carrier concentration was investigated.

Single crystals of these layered dichalcogenides can be grown easily by vapor phase transport methods. The details of the crystal growth and characterization of the samples used in this study are described in Chapter 2.

The Raman data are presented in Chapter 3 for both pure and mixed crystal systems. $\text{TiSe}_{2-x}\text{Te}_x$ mixed crystals are found to follow a one-mode behavior. $\text{TiSe}_{2-x}\text{S}_x$ and $\text{Zr}_x\text{Ti}_{1-x}\text{Se}_2$ mixed crystals are found to follow a two-mode behavior. Below the transition temperature, the zone-center phonons of the distorted state are studied as functions of x in several of the mixed crystal families, but most extensively in the $\text{TiSe}_{2-x}\text{S}_x$ system.

A discussion of the Raman data as they relate to the mixed-crystal lattice dynamics is contained in Chapter 4. Several approximations through which lattice dynamical models can be modified to describe mixed crystal behavior, including the virtual crystal approximation¹⁶ and the random element isodisplacement approximation¹⁶, are discussed. The predictions of models adapted in these approximations are compared with the experimental results.

Chapter 5 considers in some detail the proposed mechanisms for the structural phase transition in TiSe_2 . These include a band pseudo-Jahn-Teller effect³⁷, a structural distortion caused by a soft zone-boundary phonon³⁸, specific features of the band structure enhancing charge-density-wave formation^{39,40}, and

charge-density-wave formation as the crystal transforms to an excitonic insulator^{34,41,42}.

Chapter 6 summarizes the results of this investigation and proposes experiments which are of further interest. The appendices describe supplementary and related topics.

PREVIEW

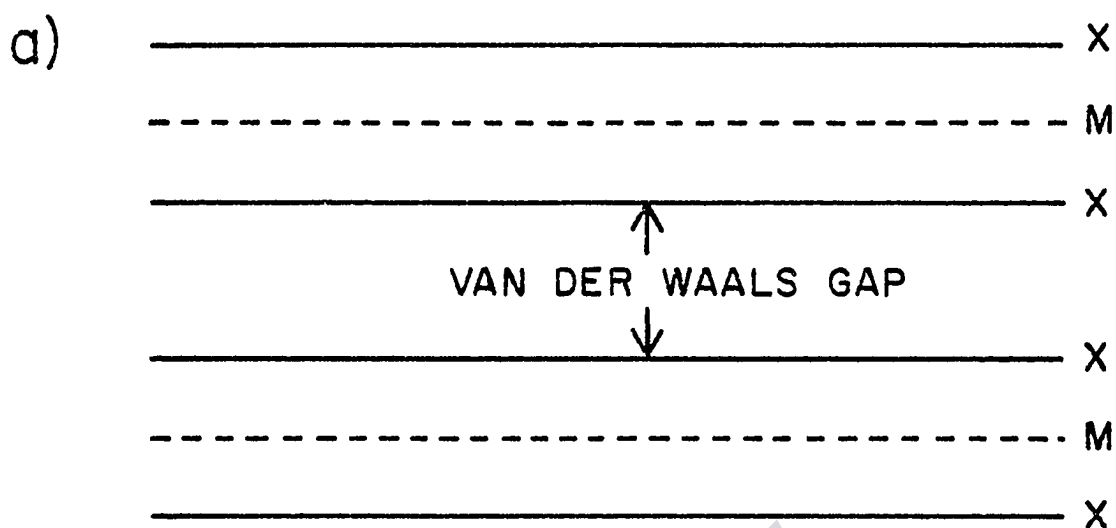
CHAPTER 2

TITANIUM DICHALCOGENIDE SAMPLES

A. Crystallography

The IVb, Vb, and VIb transition metal dichalcogenides, MX_2 , (M = transition metal, X = S, Se, or Te) form in layers which are typically separated by a gap whose thickness is nearly equal to the layer thickness⁸. (See Figure 2-1a.) The structure of each layer consists of a hexagonal net of metal atoms sandwiched between hexagonal nets of chalcogenide atoms. The coordination of the chalcogenides around the metal atoms may be either trigonal prismatic or octahedral. (See Figure 2-1b.) The layer compounds may form with a variety of stacking orders along the crystal c-axis. They are labelled 1T-, 2H-, 3R-, 4Ha-, 4Hb-, etc., polytypes⁴³ where the numbers signify the number of layers per unit cell and the letters T, H, and R identify the symmetry as trigonal, hexagonal, or rhombohedral. The lower case letters a and b denote further differences within a larger polytype group. A concise discussion of the structure of these polytypes can be found in the review article of Wilson and Yoffe⁸.

The 1T-polytype is the simplest polytype in that there is only one layer per unit cell. Figure 2-1b schematically shows the octahedral coordination that is appropriate for 1T-TiSe₂. Crystallographers refer to the structure of the 1T-polytype as the CdI₂



OCTAHEDRAL COORDINATION

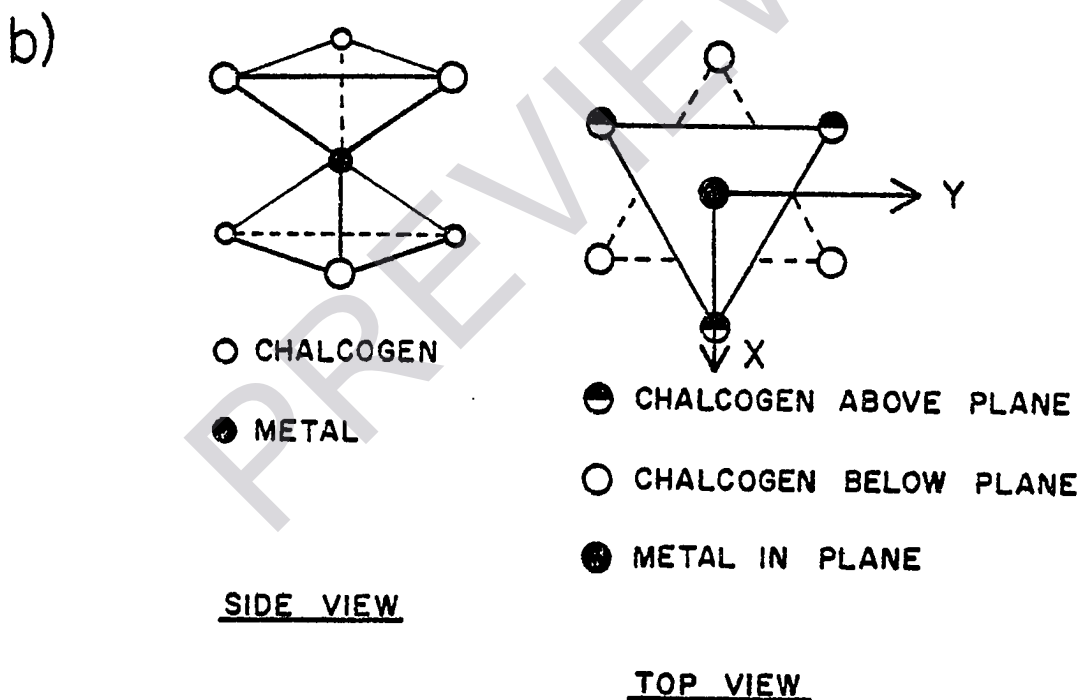


Figure 2-1 The 1T-Polytype Layered Compound

- a) Schematic of a layered compound
 b) Octahedral coordination within the layer

structure. It is related to the more three-dimensional NiAs structure adopted by many transition metal monochalcogenides⁸. For comparison, both structures are shown in Figure 2-2. Omitting alternate hexagonal nets of metal atoms of the NiAs structure results in the CdI_2 structure. The NiAs structure thus has four atoms per unit cell, whereas the CdI_2 structure has only three atoms per unit cell. Figure 2-2 illustrates in a simple way how the gap between layers arises and makes especially clear the reason for the anisotropy and two-dimensional character of the 1T-dichalcogenides. The bonding between chalcogenides across the gap in the layer structures is attributed to van der Waals interactions. Such interactions involve the attraction of one dipole to another induced by the first³. It is a weak bond and accounts for the easy cleavage of the layer compounds perpendicular to the crystal c-axis. The bonding within the layers, however, is strongly metallic or covalent. These intralayer bonds usually involve hybrid orbital configurations, intermediate between sp^2 , typical of graphite, and sp^3d^2 , the usual configuration for octahedral coordination⁸.

B. Stoichiometry

The materials studied here are mixed crystals derived from the 1T-polytype of TiSe_2 . They include $\text{TiSe}_{2-x}\text{S}_x$, $\text{TiSe}_{2-x}\text{Te}_x$, $\text{Zr}_x\text{Ti}_{1-x}\text{Se}_2$ and $\text{V}_x\text{Ti}_{1-x}\text{Se}_2$. Since the transition metal ions may exist in several oxidation states, transition metal compounds are quite prone to variations in stoichiometry⁴⁴. In fact, for many of the layer compounds, by slowly filling in the van der Waals gap,